11^{th} International Conference on Fracture Mechanics of Concrete and Concrete Structures
FraMCoS-11
J. M. Chandra Kishen, A. Ramaswamy, S. Ray and R. Vidyasagar (Eds)
https://doi.org/10.21012/FC11.092372

ACOUSTIC EMISSION CHARACTERIZATION OF 3D -PRINTED ULTRA-HIGH PERFORMANCE CONCRETE BEAMS UNDER BENDING

VAIBHAV V. INGLE*, PRABHAT R. PREM†, VIGNESH K. RAMAMURTHY * and DARSSNI RAVICHANDRAN *

*Research Fellow, CSIR-Structural Engineering Research Centre, Chennai 600 113, Tamil Nadu, India.

†Principal Scientist, CSIR-Structural Engineering Research Centre, Chennai 600 113, Tamil Nadu, India.
e-mail: prabhat@serc.res.in

Key words: 3D Concrete Printing, Ultra High-Performance Concrete, Acoustic Emission, Fiber, Coarse aggregete

Abstract. In this study, the aim is to investigate the damage evolution and crack formation within the layers of 3D-printed Ultra High-Performance Concrete (3DP-UHPC) prisms using Acoustic Emission (AE) testing. The specimens under examination include 3DP-UHPC prisms with and without coarse aggregate, tested in both lateral and perpendicular orientations relative to the printing direction. Micro steel fibers with a volume fraction of 2% are incorporated into the 3D-printed UHPC specimens to enhance the structural properties. The analysis focuses on various AE parameters such as count, duration, amplitude, and RA value (rise time to amplitude). By evaluating these parameters, the study aims to understand how they change throughout the damage progression. Notably, the influence of the direction of printing on the AE activity is also considered, indicating the potential anisotropic behavior of the 3DP-UHPC specimens.

1 INTRODUCTION

3D Concrete Printing (3DCP) is revolutionizing the industry of construction by offering faster and more efficient building processes without the need for traditional formwork. Recent advancements have showcased its transformative potential, with achievements such as modular houses, footbridges, office buildings, schools, and low-cost toilet units, all made possible through 3D printing techniques. However, there are limitations hindering wider adoption. A significant challenge is the lack of established design codes and guidelines tailored specifically for 3DCP structures. This knowledge gap restricts the confident design and construction of 3D-printed buildings, as traditional codes, are not directly applicable to the unique characteristics of 3DCP. For example, 3D-printed concrete elements exhibit anisotropic behavior, with varying strengths and stiffness in different orientations [1]. Numerous studies have highlighted that compression specimens demonstrate high strength in the direction of printing [2]. The flexural strengths perpendicular and parallel to the printing element within the printing plane are similarly high. However, the strength across the layers (perpendicular to the printing plane) is comparatively lower [3]. This also allows for flexibility in adjusting the printing mode to meet various engineering requirements by making the specimens brittle and ductile in different directions. Yang et al. [4] in terms of direction, the study found that the compressive elastic modulus showed variability, indicating anisotropic behavior. On the other hand, the tensile elastic modulus remained

relatively constant across different orientations. It is also observed that applying smaller nozzle sizes and higher fiber dosage in the mix enhances the alignment of fibers in the direction of printing and thus enhances mechanical strength [5]. Few studies propose incorporating coarse aggregate into the printing mix to mitigate the mechanical anisotropy observed in 3D-printed concrete. The optimal dosage of coarse aggregate improves interlayer bonding, while careful selection of printing parameters helps reduce trapped air bubbles, leading to a denser microstructure [6]. The experimental findings suggest that the optimal initial flowability range for printable concrete is between 178 and 200 mm. [7], and the recommended cement-to-aggregate ratio for printable concrete ranges from 0.35 to 0.60. [8]. While previous studies have provided valuable insights, a knowledge gap remains regarding the failure process and cracking behavior in anisotropic directions in 3D-printed specimens. This paper addresses this gap by conducting acoustic emission tests on 3D-printed prisms in the z and y directions. The study investigates explicitly fibered Ultra-High-Performance Concrete (UHPC) specimens, both with and without coarse aggregate. Monitoring AE activity during load testing makes it possible to assess the structural response, including the onset of microcracking, deformation, and potential failure. The AE signals can indicate the development of internal damage, detect crack initiation and propagation and provide insight into the progression of deterioration. During load testing, AE sensors are strategically placed on the surface of the 3D-printed UHPC beams. As the load is applied, the AE sensors detect and record acoustic emissions produced by the specimen. These emissions can originate from various sources, such as microcracks, crack propagation, delamination, or other internal structural changes. In the current study, we investigate the anisotropic behavior of 3DP -UHPC specimens. The details of the same are expanded hereafter.

2 METHODOLOGY

2.1 Mix design

Two types of 3D-UHPC mix, namely UHPC-F, and UHPC-FCA, are utilized to fabricate prisms in this study. Both mixes have the same binder, aggregate content, and fiber dosage (2% by volume). However, there is a distinction in the size of the aggregates used. The 3D-UHPC-F mixes consist of fine aggregate with a size smaller than 2 mm, while the 3D-UHPC-FCA mixes incorporate coarse aggregate ranging from 5 mm to 6 mm in size. More details of the mix design and rheological properties is available in [7, 9].

Figure 1: Typical test set up

2.2 Testing and instrumentation

The experimental configuration is illustrated in Fig.1. The specimens undergo displacement-controlled testing at a loading rate of 0.2 mm/min. Similar prisms are tested in the Z-direction (orthogonal to the direction of printing) and the Y-direction (lateral direction to the printing). The beams are subjected to testing until softening behavior becomes evident. An 8-Channel PCI-Express Bus AE system is employed as the measuring system. Six R6I-AST sensors are utilized, which possess a peak sensitivity of 117 dB, an operating frequency range

of 40-100 kHz, and a resonant frequency of 55 kHz. Using silicone grease as a coupling agent, these sensors are firmly placed on the specimen surface to capture AE signals. It is set to 40 dB for the pre-amplifier gain. The sensitivity and coupling of the AE sensors are determined using a Hsu-Nielsen source (pencil-lead break). A similar strategy is adopted in previous studies [10, 11]

3 Results and Discussion

3.1 Source localization

Figure.2, and Fig.3 illustrate the typical failure pattern observed in the tested specimens. By utilizing source localization techniques, we aim to determine the location of the AE events or specimen failures, as depicted in Fig.4, and Fig.5. The examination of these localized events allows us to analyze the differences that arise due to anisotropy within the specimens.

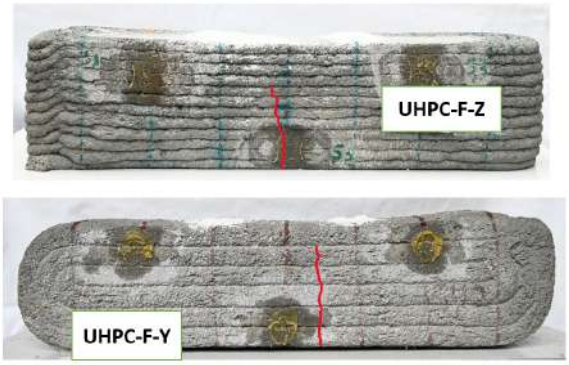

Figure 2: Failure pattern in UHPC-FM

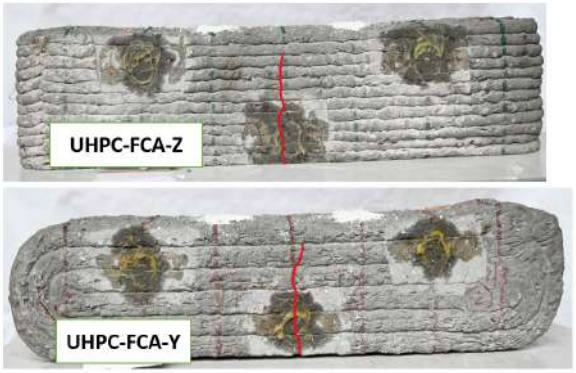

Figure 3: Failure pattern in UHPC-FCA

The source localization method relies on measuring the arrival times of P-waves using multiple AE transducers. Typically, four transducers are used for 2D analysis, while six to eight transducers are used for 3D analysis. In this particular study, six AE sensors are mounted on the specimens for 3D localization shown in Fig.1. To measure the wave propagation velocity in UHPC specimens, pencil lead tests are conducted following the guidelines of ASTM E976-15. For localization, a triangulation algorithm with a homogeneous velocity profile is employed. The 3D localization of AE sources is achieved using the iterative gradient method. Various algorithms, such as the Nelder-Mead Algorithm or Geiger 3D, can be utilized for 3D localization. To enhance the accuracy of the localization, an edge enhancement filter is employed to sharpen the arrival time of the first P-waves. The crack's location is determined using the wave velocity in the material and the time difference between the two registered AE signals, according to the underlying principle. [12]. Based on the observations depicted in Fig.2, and Fig.3 it can be noted that all the tested beams exhibited failure due to the development of a single dominant crack.

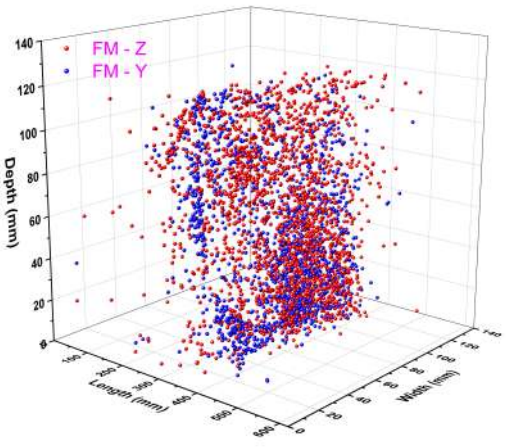

Figure 4: Maps of acoustic emission (AE) events for UHPC-F

Maps of acoustic emission (AE) events for UHPC-F and UHPC-CA beams, tested in the Z and Y directions, are illustrated in Fig.4 and

Fig.5 respectively. It is worth mentioning that no notable disparity is observed in the occurrence of AE events when the beams were tested in either the Z or Y direction. However, the number of AE events recorded in UHPC-CA beams is higher compared to the corresponding UHPC beams.

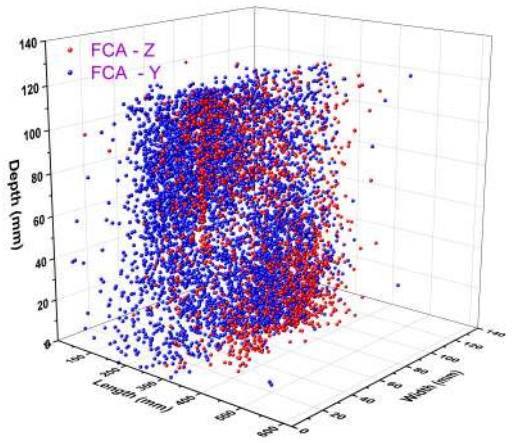

Figure 5: Maps of acoustic emission (AE) events for UHPC-CA beams

3.2 Crack classification

Clustering is employed to differentiate between sources originating from different origins and better understand the relationships among key mechanisms such as elastic behavior, matrix cracking, fiber breaking, and fiber pull-out in the case of concrete [10]. Generally, concrete cracks can be divided into two primary categories.: shear cracks and tensile cracks. [13], and this can be improved based on K-means [8]. K-means clustering involves organizing data into clusters, initializing centroids, assigning data points to the nearest centroid, updating centroids based on cluster memberships, and iterating until convergence is achieved or the centroids remain unchanged. The difference between centroids is commonly used to assess the distance between clusters.

The classification of cracks in concrete into shear and tensile modes can be achieved by clustering data obtained from the plot of RA value and Average Frequency (AF). The RA value is derived from the ratio of rise time to amplitude, where the rise time represents the duration for the AE signal to increase from a threshold level to its peak, and the amplitude indicates the signal's maximum value. The RA value reflects the sharpness or steepness of crack development. Similarly, the AF value is obtained by dividing the count of acoustic emission events by the duration over which these events occur. The AF value provides insights into the frequency content of the acoustic emission signals. This study calculated the RA and AF values using a moving average of 100 consecutive hits. Through RA and AF analysis, different cracking modes, namely tensile crack and shear cracking, can be distinguished. Shear crack waveforms exhibit higher RA values and lower AF values, while tensile crack waveforms display lower AF values and shorter RA values. Typical plots of K-mean clustering for 3DC printed beam of UHPC-FCA and UHPC-F in Z and Y beam testing direction are shown in Fig.6, Fig.7, and Fig.8, Fig.9 respectively.

RILEM Recommendation [13]states that AE signals can be analyzed during testing to detect active cracks, such as tensile cracks, and other forms like shear cracks. In order to accurately identify and localize active cracks, the test must be performed in such a way that it does not significantly impair the structure's functionality. However, in this study, we have identified distinct range values for RA and AF that correspond to shear and tension cracks in 3D-printed beams tested in the Z and Y printing orientation. These range values are presented in Table no. 1 for UHPC-F printed beams and Table no. 2 for UHPC-FCA printed beams. The results of the study revealed that there is a higher range of rise angle (RA) value in the Z direction compared to the Y direction for UHPC-F printed beams. Conversely, a reverse trend is observed for the average frequency (AF) in tension cracks, indicating lower values in the Z direction compared to the Y direction. These trends are similarly observed in shear cracks as well. In the case of UHPC-FCA printed beams, it is observed that there are higher ranges of RA values and AF in the Y direction compared to the Z direction for

tensile cracks. Conversely, for shear cracks, the range of RA values is found to be higher in the Y direction than in the Z direction.

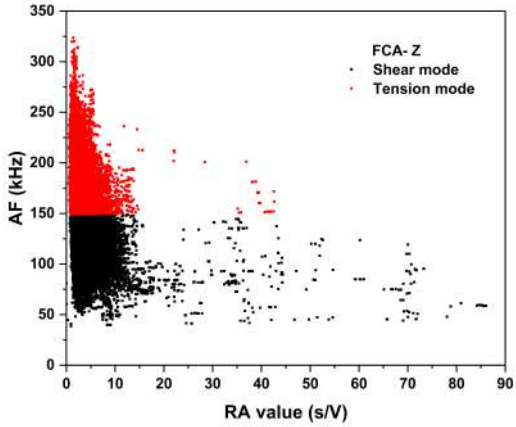

Figure 6: Clustering of FCA-Z.

Furthermore, it is observed that the Average Frequency (AF) exhibited a higher range in the Z direction when compared to the Y direction.

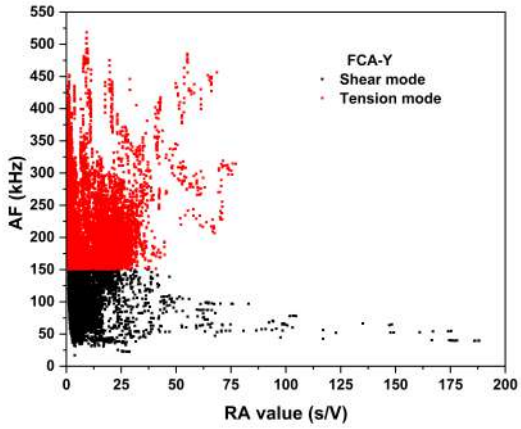

Figure 7: Clustering of FCA-Y.

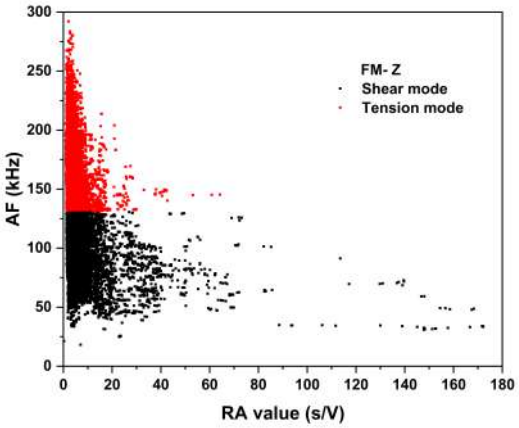

Figure 8: Clustering of FM-Z.

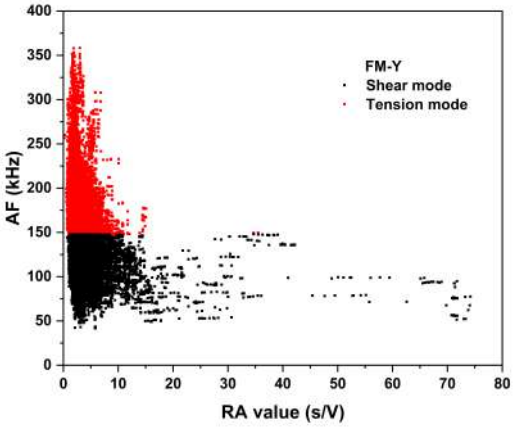

Figure 9: Clustering of FM-Y.

Table 1: UHPC-F: Crack Classfication

	Tensile crack	
	Z	Y
RA	2.14-3.79	0.05-2.87
AF	157.65-292.10	180.68-500
	Shear crack	
RA	5.64-174.02	4.01-5.84
AF	33.66-102.374	41.61-114.79

Table 2: UHPC-F-CA: Crack Classfication

	Tensile crack	
	Z	Y
RA	1.41-2.79	6.66-9.24
AF	179.11-323.62	191.76-518.37
	Shear crack	
RA	4.02-69.49	4.82-192.11
AF	43.76-119.53	39.63-109.54

4 Conclusion

The present study examined the Acoustic Emission characteristics in flexural behavior of 3D-printed UHPC (Ultra-High-Performance Concrete) beams. The bending behavior of the printed beams is evaluated in (i) two directions: perpendicular to the printing direction and laterally. Additionally, UHPC specimens are printed with and without coarse aggregate, incorporating fibers into the mix. Through source localization studies, we did not observe any interlayer delamination in the printed beams. Acoustic emission parameters are analyzed using the K-means algorithm to identify tension and shear cracks. During testing, more acoustic emission events are observed for 3DP-UHPC specimens with coarse aggregate. Shear cracks are predominantly observed in the Z-direction for UHPC-F, while tension cracking are more prevalent in the Y-direction. Similarly, for UHPC-FCA, shear cracking is dominant in the Z-direction, while tension cracking is observed to be dominant in the Y-direction.

REFERENCES

[1] Kaliyavaradhan, S. K., Ambily, P. S., Prem, P. R., & Ghodke, S. B. (2022). Test methods for 3D printable concrete. *Automation in Construction*, 142, 104529.

[2] Ding, T., Xiao, J., Zou, S., & Zhou, X. (2020). Anisotropic behavior in bending of 3D printed concrete reinforced with fibers. *Composite Structures*, 254, 112808.

[3] Murcia, D. H., Genedy, M., & Taha, M. R. (2020). Examining the significance of infill printing pattern on the anisotropy of 3D printed concrete. *Construction and Building Materials*, 262, 120559.

[4] Yang, Y., Wu, C., Liu, Z., Wang, H., & Ren, Q. (2022). Mechanical anisotropy of ultra-high performance fibre-reinforced concrete for 3D printing. *Cement and Concrete Composites*, 125, 104310.

[5] Arunothayan, A. R., Nematollahi, B., Ranade, R., Bong, S. H., Sanjayan, J. G., & Khayat, K. H. (2021). Fiber orientation effects on ultra-high performance concrete formed by 3D printing. *Cement and Concrete Research*, 143, 106384.

[6] Wang, X., Jia, L., Jia, Z., Zhang, C., Chen, Y., Ma, L., ... & Zhang, Y. (2022). Optimization of 3D printing concrete with coarse aggregate via proper mix design and printing process. *Journal of Building Engineering*, 56, 104745.

[7] Greeshma Giridhar, Prabhat Ranjan Prem & Shankar Kumar . 2023. Development of concrete mixes for 3D printing using simple tools and techniques *Sadhana*

[8] Chen, Y., Zhang, Y., Pang, B., Liu, Z., & Liu, G. (2021). Extrusion-based 3D printing concrete with coarse aggregate: Printability and direction-dependent mechanical performance. *Construction and Building Materials*, 296, 123624

[9] Ravichandran, D., Giridhar, G., kumar Ramamurthy, V., & Prem, P. R. (2023). Influence of test protocol on determining the rheological properties of cement pastes mixtures for concrete 3D printing. *Materials Today: Proceedings*.

[10] Prem, P. R., Murthy, A. R., & Verma, M. (2018). Theoretical modelling and acoustic emission monitoring of RC beams strengthened with UHPC. *Construction and Building Materials*, 158, 670-682.

[11] Prem, P. R., Verma, M., & Ambily, P. S. (2021, April). Damage characterization of reinforced concrete beams under different failure modes using acoustic emission. *Structures* Vol. 30, pp. 174-187.

[12] Maria Strantzaa, Danny Van Hemelrijck, Patrick Guillaume, Dimitrios G. Aggelis. 2017. Acoustic emission monitoring of crack propagation in additively manufactured and conventional titanium components. *Mechanics Research Communications*, 84, 8-13.

[13] Masayasu Ohtsu.,kumamoto-u. ac. jp. (2010). Recommendation of RILEM TC 212-ACD: acoustic emission and related NDE techniques for crack detection and damage evaluation in concrete* Test method for damage qualification of reinforced concrete beams by acoustic emission. *Materials and structures*, 43(9), 1183-1186.